Combinatorial Search for Improved Metal Oxide Oxygen Evolution Electrocatalysts in Acidic Electrolytes

ARTICLE · JANUARY 2013

DOI: 10.1021/co300086h · Source: PubMed

3 AUTHORS, INCLUDING:

Bruce A Parkinson
University of Wyoming
251 PUBLICATIONS **7,094** CITATIONS

ACS Combinatorial Science

Research Article

pubs.acs.org/acscombsci

Combinatorial Search for Improved Metal Oxide Oxygen Evolution Electrocatalysts in Acidic Electrolytes

David Seley,[†] Katherine Ayers,[‡] and B. A. Parkinson*,[†]

[†]Department of Chemistry and School of Energy Resources, University of Wyoming, Laramie, Wyoming 82071, United States

[‡]Proton OnSite, 10 Technology Drive, Wallingford, Connecticut 06492, United States

Supporting Information

ABSTRACT: A library of electrocatalysts for water electrolysis under acidic conditions was created by ink jet printing metal oxide precursors followed by pyrolysis in air to produce mixed metal oxides. The compositions were then screened in acidic electrolytes using a pH sensitive fluorescence indicator that became fluorescent due to the pH change at the electrode surface because of the release of protons from water oxidation. The most promising materials were further characterized by measuring polarization curves and Tafel slopes as anodes for water oxidation. Mixed metal oxides that perform better than the iridium oxide standard were identified.

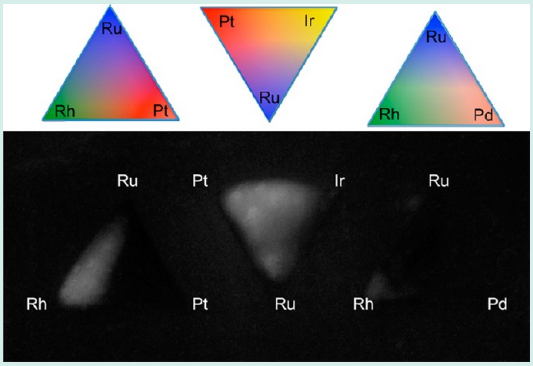

KEYWORDS: *electrocatalysts, PEM, electrolysis, anode, combinatorial, metal oxides*

INTRODUCTION

Water electrolysis is being considered as a possible method for storage of renewable electricity to both supply hydrogen as fuel and to store the electrical energy from wind and solar energy for times when the wind or sun is unavailable. To make electrolysis a viable energy storage option, its efficiency must be improved and its cost must be reduced as much as possible. Most of the electrocatalysts used for oxygen generation in an electrolysis cell are metal oxides with high precious metal content. An obvious cost reduction strategy would be to replace some or all of these metals with cheaper and more abundant metals. Since multiple ratios of many metals need to be produced and tested, a combinatorial method for rapidly producing and screening multiple component metal oxides for catalytic activity for the electrooxidation of water is developed. Libraries of metal oxide compositions were prepared using ink jet printing of metal oxide precursors, similar to what we reported earlier for producing and screening metal oxide semiconductors for solar water photoelectrolysis.[1,2] In that previous work photocurrent was used to screen for activity, whereas in this study we adopted a technique based on pH changes, expected at the electrode surface because of the release of protons in the water oxidation reaction, that produces fluorescence in a pH sensitive fluorescence indicator. This approach was used by Reddington et al.,[3] who investigated precious metals for catalytic methanol oxidation for fuel cell applications.

This combinatorial study focuses on anode materials for water electrolysis for proton exchange membrane (PEM) electrolyzers that operate under acidic conditions. The two most commonly used metal oxides based on their catalytic ability to oxidize water are IrO_2 and RuO_2.[4] RuO_2 is considered to be most catalytic, but it is unstable at potentials greater than 1.4 V vs NHE.[5] IrO_2 and PtIr oxide blends are commonly used for electrolysis of water, but are less active than RuO_2. Several stabilized metal oxide combinations have been investigated. RuO_2 has been stabilized using IrO_2 or Pt.[6,7] RuO_2 has also been mixed with Ir/Sn, Ir/Ta, Sn, and Sb-doped Sn oxides to help stabilize the electrode.[8−10] Mixed metal oxides of IrO_2 have also been prepared using Sn, Pt, and Sn/Nb.[11−14] Combinatorial approaches to finding superior mixed platinum group metal electrocatalysts for water oxidation under acidic conditions have been undertaken by Dokoutchaev and Chen.[15,16] Dokoutchaev looked strictly at water oxidation electrocatalysts, while Chen was looking for bifunctional catalysts for oxygen reduction and water oxidation. More recently, Gerken et al. used a combinatorial approach to find mixed metal oxide electrocatalysts for water oxidation under basic conditions.[17] These previous works include combinatorial studies on metals alone in acidic conditions, or metal oxides in basic conditions. What is lacking is a study that involves mixed metal oxides in acidic conditions. In this report, two approaches were taken to investigate mixed metal oxide electrocatalysts. Our first approach was to take the base metals Mn, Nb, Al, and Sn as structural stabilizers with the addition of the more catalytic elements, Ir and Ru. Al, Sn, and Nb are metals that are

Received: August 9, 2012
Revised: November 12, 2012
Published: January 8, 2013

   dx.doi.org/10.1021/co300086h | ACS Comb. Sci. 2013, 15, 82−89

expected to stabilize the catalytic metal oxides in acidic conditions.[9] Mn was chosen because of its stability in strongly acidic conditions.[12b] The second approach involved mixing the platinum group metals (PGMs) to investigate whether mixtures of the less expensive PGMs (Pd and Ru), with the more expensive and more catalytic PGMs, could improve or maintain their catalytic activity. All of these PGM oxides are considered to be very stable in acidic conditions and most are very conductive, a useful property of a good electrocatalyst.[4]

EXPERIMENTAL SECTION

The electrodes were printed using a Dimatix materials ink jet printer previously described[1,2] on 3" × 3" glass plates with a fluorine-doped tin oxide (FTO) conductive coating. Discrete ternary compositions of Ir, Ru were printed and the structural component when using base metals. Three mm by three mm arrays of 20 to 64 squares were printed on FTO, varying the compositions at each square. The solutions used for printing the structural metals were $Mn(NO_3)_2$, $Al(NO_3)_3$, $SnCl_2$, and $NH_4NbO(C_2O_4)_2$. All structural metal concentrations were 0.1 M in our "ink" mixture containing water and glycols. The PGM Ir and Ru metal salts were $RuCl_3$ and $(NH_4)_2IrCl_6$ in concentrations of 0.05 M based on the solubility of the precursor salts.

For compositions involving platinum group metals as the structural stabilizing component, gradients of each of the metals were printed as seen in Figure 1a. The other PGMs used and

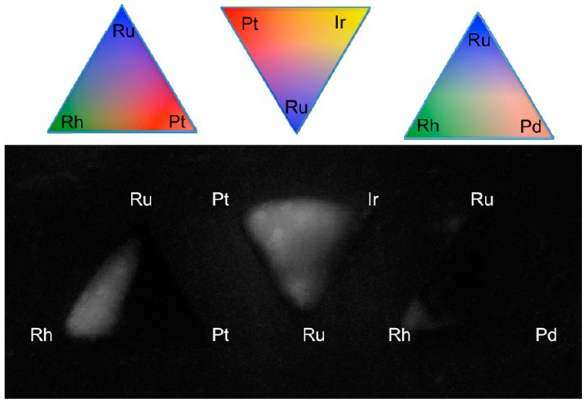

Figure 1. Fluorescence image of gradient mixtures containing platinum group metals in an electrolyte containing 15 wt.% PVA. Six other similar gradient mixtures were also printed and screened.

their concentrations loaded into the ink jet cartridges were as follows: H_2PtCl_6, 0.05 M; $Pd(NO_3)_2$ 0.05 M; and $RhCl_3$, 0.05 M. All printed metal precursors were fired in air at 525 °C for 1 h to convert them to the corresponding metal oxides. Once these gradients were screened, discrete compositions of promising mixed metal oxides of the PGMs were then printed and rescreened for comparison.

The half-reaction at the anode for the electrolysis of water in acidic conditions is shown in eq 1 and produces four protons near the electrode surface for every oxygen molecule produced.

$$2H_2O \rightarrow O_2 + 4H^+ + 4e^- \qquad E^\circ = 1.23\ V \qquad (1)$$

The screening method chosen uses a pH sensitive fluorescence indicator described by Reddington[3] and Dokoutchaev,[15] who investigated catalytic metals for methanol oxidation in fuel cells and water oxidation, respectively. The fluorescent pH indicator is 3-(2′-pyridyl)-[1,2,3]-triazolo[1,5-a]pyridine, (PTP), and was synthesized by following a literature procedure.[18] The electrolyte solution contained 0.5 M $NaClO_4$, and the pH was adjusted to about 3.5 before screening using $HClO_4$. The intensity of fluorescence of the indicator increases in highly acidic solutions and shows a maximum around pH 2. As seen in the above reaction, protons are released during the oxidation of water, thereby changing the local pH at the active electrodes surfaces. During a typical screening experiment, the initial potential was 1.2 V vs NHE and then increased in 33 mV steps every 3 min until fluorescence was observed under illumination from a hand-held UV-lamp. Images of the fluorescence were taken with a digital camera using a 420 nm band-pass filter. The first images were taken at the onset of fluorescence and then every 10 to 15 s thereafter. The catalysts fluorescing first (i.e., the first 4 or 5) were selected for further studies. If fluorescence of multiple catalysts (greater than 5) were nearly simultaneous, then all were included for further study. The fluorescence in aqueous solution is relatively weak and would become more diffuse with time because of proton diffusion, and so polyvinyl alcohol (PVA, 15% by weight) was added to the electrolyte. The higher viscosity solution containing the PVA helps to slow the diffusion of protons and fluorescing protonated dye away from the electrode surface, thereby enhancing the contrast in the digital photographic images. Similar results were obtained without adding the PVA. Comparison of current−voltage curves of the aqueous indicator solution and the indicator solution having the PVA additive showed similarly shaped curves. The current densities of the PVA additive solutions were lower than those of the aqueous solution, which is expected because of the increased viscosity of the PVA additive solution. Images in which PVA was used will be noted in the figure caption.

Electrochemical current voltage studies were performed using a 3-electrode cell with a Ag/AgCl reference electrode and a graphite rod as the counter electrode. The working electrode was a 1 cm^2 mixed metal salt printed on FTO and fired under the same conditions as the screening compositions. The electrolyte was 0.5 M H_2SO_4. It is likely that the catalysts behave somewhat differently in a 0.5 M H_2SO_4 solution vs a solution with a pH of 3. However, the pH 3 solution used in the screening experiments is the lowest pH at which reasonable results using a fluorescent indicator can be expected. Although traditional electrochemical experiments are superior for assessing the electrocatalytic properties of materials, the optical screening method is a much quicker approach to evaluating large combinations of materials. All electrochemical experiments were conducted at room temperature. The initial potential was 1.40 vs NHE and was increased in 5 mV increments every 1 min to a final potential of 1.65 V vs NHE with the current monitored. The currents were measured every second and then a 60-point average was calculated and plotted against the potential.

RESULTS AND DISCUSSION

Combinatorial Screening. Figure 1 illustrates the screening experiments for gradient compositions of the PGMs. Electrochemical experiments were performed to verify that the different electrolytes, containing PVA or not, did not have an effect on the catalytic activity or current densities of the materials screened. The triangular features shown represent ternary compositions such that at each vertex, the pure metal oxide exists and decreases in concentration as you move away

dx.doi.org/10.1021/co300086h | ACS Comb. Sci. 2013, 15, 82−89

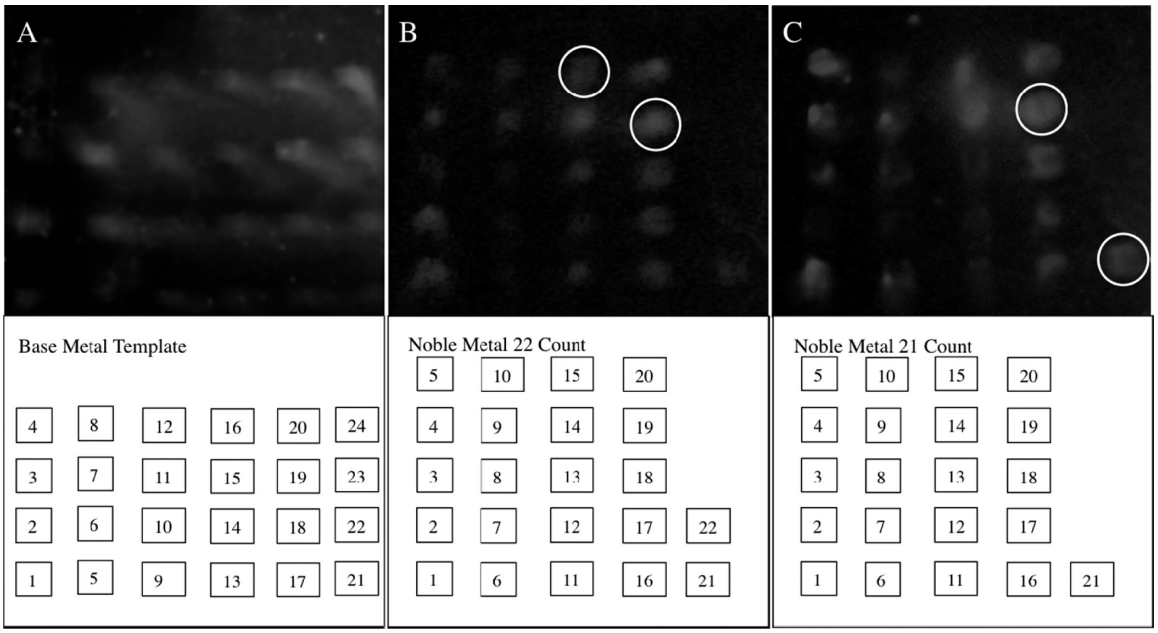

Figure 2. Fluorescence images of discrete compositions of aluminum, iridium and ruthenium mixed metal oxides (A) at a potential of about 1.4 V vs NHE, and platinum group metals (B and C) at potentials close to 1.3 V vs NHE. The PGM compositions were made after screening gradients. The mole percent of each composition is given in Table 1.

Table 1. Compositions of Mixed Metal Oxides Screened

		Base Metal Template[a]		
1 $Ir_{0.32}M_{0.65}Ru_{0.03}$	6 $Ir_{0.70}M_{0.28}Ru_{0.02}$	11 $Ir_{0.61}M_{0.30}Ru_{0.09}$	16 $Ir_{0.84}M_{0.11}Ru_{0.05}$	21 $Ir_{0.49}M_{0.43}Ru_{0.08}$
2 $Ir_{0.51}M_{0.45}Ru_{0.04}$	7 $Ir_{0.80}M_{0.17}Ru_{0.03}$	12 $Ir_{0.70}M_{0.20}Ru_{0.10}$	17 $Ir_{0.30}M_{0.60}Ru_{0.10}$	22 $Ir_{0.65}M_{0.25}Ru_{0.10}$
3 $Ir_{0.63}M_{0.32}Ru_{0.05}$	8 $Ir_{0.86}M_{0.11}Ru_{0.03}$	13 $Ir_{0.51}M_{0.46}Ru_{0.03}$	18 $Ir_{0.44}M_{0.40}Ru_{0.16}$	23 $Ir_{0.73}M_{0.16}Ru_{0.11}$
4 $Ir_{0.73}M_{0.21}Ru_{0.06}$	9 $Ir_{0.32}M_{0.63}Ru_{0.05}$	14 $Ir_{0.69}M_{0.27}Ru_{0.04}$	19 $Ir_{0.54}M_{0.27}Ru_{0.19}$	24 $Ir_{0.78}M_{0.10}Ru_{0.12}$
5 $Ir_{0.52}M_{0.46}Ru_{0.02}$	10 $Ir_{0.49}M_{0.44}Ru_{0.07}$	15 $Ir_{0.78}M_{0.17}Ru_{0.05}$	20 $Ir_{0.61}M_{0.17}Ru_{0.22}$	
		Noble Metal 22 Count Template		
1 $Ir_{0.40}Pt_{0.50}Rh_{0.10}$	6 $Ir_{0.20}Pt_{0.30}Rh_{0.50}$	11 $Ir_{0.30}Rh_{0.70}$	16 $Ir_{0.50}Pt_{0.40}Rh_{0.10}$	21 $Ir_{0.50}Pt_{0.50}$
2 $Ir_{0.30}Pt_{0.50}Rh_{0.20}$	7 $Ir_{0.30}Pt_{0.20}Rh_{0.50}$	12 $Rh_{0.70}Ru_{0.30}$	17 $Ir_{0.50}Pt_{0.30}Rh_{0.20}$	22 $Pt_{0.50}Pd_{0.50}$
3 $Ir_{0.10}Pt_{0.50}Rh_{0.40}$	8 $Ir_{0.25}Pt_{0.25}Rh_{0.50}$	13 $Rh_{0.80}Pt_{0.20}$	18 $Ir_{0.50}Pt_{0.25}Rh_{0.25}$	
4 $Ir_{0.20}Pt_{0.50}Rh_{0.30}$	9 $Ir_{0.30}Pt_{0.10}Rh_{0.60}$	14 $Rh_{0.80}Pd_{0.20}$	19 $Ir_{0.60}Rh_{0.40}$	
5 $Ir_{0.30}Pt_{0.70}$	10 $Ir_{0.20}Pt_{0.10}Rh_{0.70}$	15 Ir	20 $Ir_{0.50}Rh_{0.50}$	
		Noble Metal 21 Count Template		
1 $Ir_{0.33}Rh_{0.33}Ru_{0.33}$	6 $Ir_{0.60}Rh_{0.30}Pd_{0.10}$	11 $Pt_{0.60}Ir_{0.20}Ru_{0.20}$	16 $Rh_{0.80}Ru_{0.10}Pd_{0.10}$	21 Ir
2 $Ir_{0.30}Pt_{0.60}Pd_{0.10}$	7 $Ir_{0.60}Rh_{0.10}Ru_{0.30}$	12 $Pt_{0.70}Ir_{0.10}Ru_{0.20}$	17 $Rh_{0.90}Ru_{0.05}Pd_{0.05}$	
3 $Ir_{0.40}Pt_{0.50}Pd_{0.10}$	8 $Ir_{0.70}Ru_{0.20}Pd_{0.10}$	13 $Pt_{0.80}Ir_{0.10}Ru_{0.10}$	18 $Ir_{0.42}Ru_{0.28}Pt_{0.10}Rh_{0.20}$	
4 $Ir_{0.5}Rh_{0.20}Ru_{0.30}$	9 $Ir_{0.70}Rh_{0.20}Pd_{0.10}$	14 $Rh_{0.70}Ru_{0.20}Pt_{0.10}$	19 $Ir_{0.42}Ru_{0.28}Pt_{0.05}Rh_{0.25}$	
5 $Ir_{0.50}Rh_{0.10}Ru_{0.40}$	10 $Ir_{0.80}Ru_{0.10}Pd_{0.10}$	15 $Rh_{0.80}Ru_{0.10}Pt_{0.10}$	20 $Ir_{0.42}Ru_{0.28}Pt_{0.15}Rh_{0.15}$	

[a]M = Al, Nb, Mn, Sn.

from the vertex, going to zero just before the opposite edge. Each edge of each triangle, therefore, represents a binary compound whose concentration varies in the two metal oxides along the edge. As seen in the images, fluorescence is apparent in the Rh rich area of the Ru/Pt/Rh triangle and most of the Ru/Pt/Ir triangle with only a small fluorescence observed in the Rh corner of the Ru/Pd/Rh triangle. Two triangles contain a Ru/Rh binary edge, but appear to be fluorescing with different intensities. It is likely that this is an artifact of the materials mixing to some extent during the pyrolysis step. It appears that Pd has a deleterious effect on the catalytic properties of the Ru/Rh edge, whereas Pt appears to enhance catalysis.

Discrete Composition Screening. Figure 2 shows screening experiments of patterns with distinct compositions. Each image represents a different set of compositions. Figure 2A shows 24 different distinct compositions containing Al, Ru, and Ir in various proportions. The bottom row of Figure 2A consists of compositions in which the Al concentration is between 40 and 65 mol percent. These compositions are difficult to discern in the figure based on the lack of fluorescence, hence lack of activity. Figures 2B and 2C are only PGMs and also contain a composition consisting only of IrO_2, which was used as a standard. The IrO_2 standard and an additional mixed metal oxide composition are highlighted in both 2B and 2C. These images show that the $Ir_{0.60}Rh_{0.40}$ (box 19 in 2B) and $Ir_{0.42}Ru_{0.28}Pt_{0.05}Rh_{0.25}$ (box 19 in 2C) compositions in both produce a greater fluorescence in the solution than the IrO_2 (box 15 in 2B and box 21 in 2C) standards.

dx.doi.org/10.1021/co300086h | ACS Comb. Sci. 2013, 15, 82−89

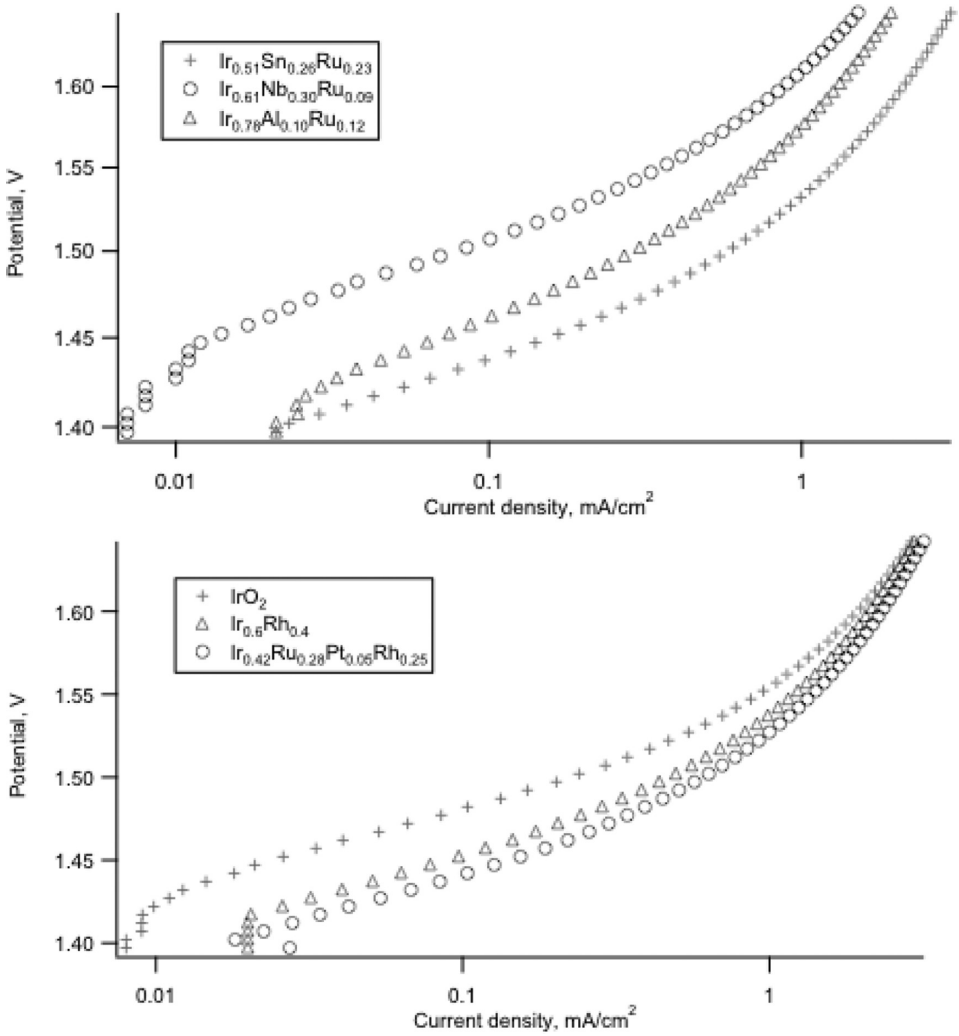

Figure 3. Polarization curves of the best performing base metal compositions (A) and PGM compositions (B).

The compositions for each of the features shown in Figure 2 are provided in Table 1. The compositions for the base metals (Al, Nb, Sn) are virtually the same for each metal tested. The Al compositions shown indicate that the largest numbers of protons produced come from compositions in which Al is 27 mol percent or less. The Mn compositions fluoresced quite early relative to the IrO_2 standards, but visual inspection of the electrodes after screening indicated the electrodes had decomposed. The screening experiments for the Nb compositions indicated that up to 44 mol percent of Nb could be present and still produce good fluorescence in solution. The greatest fluorescence from the Sn compositions originated from mixtures containing no more than 30 mol percent of Sn.

Electrochemical Characterization. Polarization curves for the best performing base metal compositions, as well as the PGM compositions identified in Figure 2, are shown in Figure 3, with the potentials reported vs NHE. The polarization data for the base metal compositions (Figure 3A) do not compare favorably to IrO_2, with the exception of the Sn composition. The current density of IrO_2 at 1.6 V is about 3 mA/cm^2. The Nb composition has a current density of about 1.5 mA/cm^2 at the same potential, and the Al composition has a current density of about 1.9 mA/cm^2. The Sn composition has a current density of about 3 mA/cm^2 at 1.6 V.

The data show that the PGM compositions (Figure 3B) have significantly higher current densities at low overpotentials than the pure IrO_2 standard. For example, at a potential of 1.46 V, the $Ir_{0.42}Ru_{0.28}Pt_{0.05}Rh_{0.25}$ oxide composition has a current density of 0.186 mA/cm^2, and the $Ir_{0.6}Rh_{0.4}$ oxide composition has a current density of 0.119 mA/cm^2, whereas the pure IrO_2 standard has a current density of 0.033 mA/cm^2. The current voltage data validates the use of fluorescence for screening these compositions since they exhibited greater fluorescence than the IrO_2 standard that was printed on the same substrate. In other words, at low current densities the number of protons generated at the surface of these different compositions is higher than the number of protons generated on the IrO_2 electrode surfaces. This may be indicative of a different water oxidation mechanism occurring on the IrO_2 surface than on the mixed metal oxides composition surfaces. The polarization curves also appear to exhibit a change in Tafel slope between lower current densities and higher current densities and appear to coalesce at current densities of greater than about 2 mA/cm^2.

Mechanism Analysis. Several different multistep mechanisms have been proposed for the electrolysis of water on metal oxides in acid. Two frequently cited mechanisms are the electrochemical oxide path and the oxide path.[19]

dx.doi.org/10.1021/co300086h | ACS Comb. Sci. 2013, 15, 82−89

Table 2. Tafel Slopes of Selected Materials

material	Tafel slope (1.49 V−1.53 V)	Tafel slope (1.59 V−1.64 V)	potential, 1 mA/cm^2 (V)
IrO_2	96 mV/decade	44 mV/decade	1.552
[b]$Ir_{0.20}Pt_{0.10}Rh_{0.70}$	95 mV/decade	45 mV/decade	1.547
[b]$Ir_{0.25}Pt_{0.25}Rh_{0.50}$	89 mV/decade	47 mV/decade	1.547
[a]$Ir_{0.60}Rh_{0.40}$	79 mV/decade	50 mV/decade	1.537
[a]$Ir_{0.42}Ru_{0.28}Pt_{0.05}Rh_{0.25}$	75 mV/decade	49 mV/decade	1.532
$Ir_{0.51}Sn_{0.26}Ru_{0.23}$	83 mV/decade	54 mV/decade	1.532

[a]Indicates compositions exhibiting greater fluorescence than IrO_2 standard. [b]Indicates compositions showing greater apparent stability than IrO_2 standard and lower potentials at high current densities.

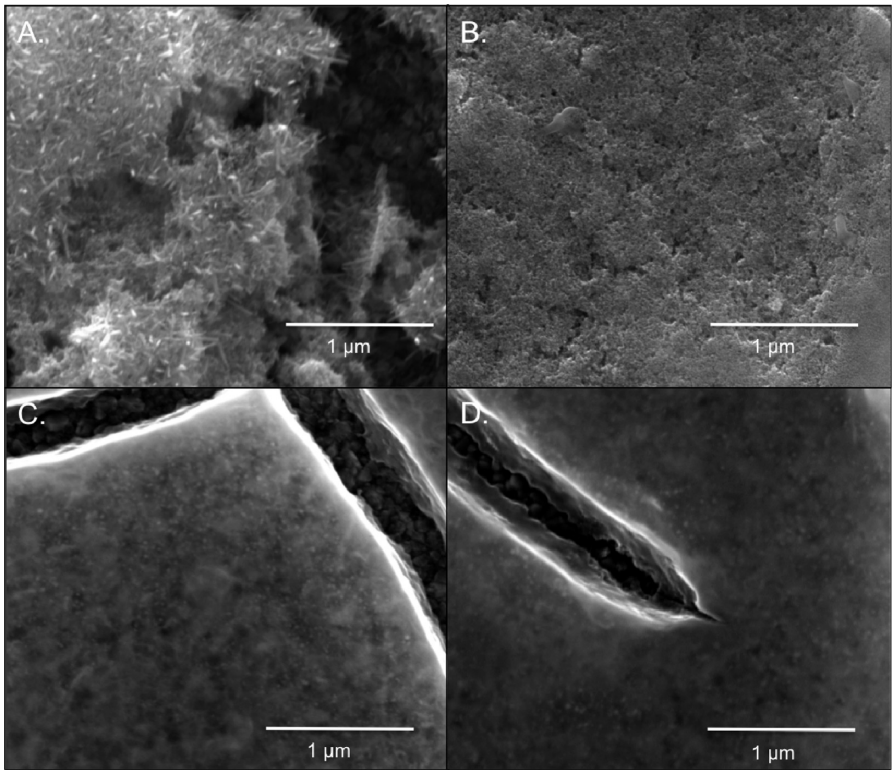

Figure 4. SEM images of mixed metal oxide electrodes; shown are those for (A) IrO_2; (B) $Pt_{0.50}Pd_{0.50}$; (C) $Ir_{0.42}Ru_{0.28}Pt_{0.05}Rh_{0.25}$; (D) $Ir_{0.20}Pt_{0.10}Rh_{0.70}$.

Electrochemical oxide path

$$S + H_2O \rightleftharpoons S{-}OH + H^+ + e^- \qquad 120\ mV$$

$$S{-}OH \rightleftharpoons S{-}O + H^+ + e^- \qquad 40\ mV$$

$$2S{-}O \rightarrow 2S + O_2 \qquad 15\ mV$$

Oxide path

$$S + H_2O \rightleftharpoons S{-}OH + H^+ + e^- \qquad 120\ mV$$

$$2S{-}OH \rightleftharpoons S{-}O + S + H_2O \qquad 30\ mV$$

$$2S{-}O \rightarrow 2S + O_2 \qquad 15\ mV$$

The first step in each of these paths is the discharge of water, an electrochemical step having a theoretical Tafel slope of about 120 mV/decade. Tafel slopes were measured at very low overpotentials in the polarization curves for several compositions. The results are presented in Table 2. Tafel slopes were also measured at an intermediate overpotential range, and this data is also presented for several compositions.

The data show that the two PGM compositions exhibiting greater fluorescence than the IrO_2 standard highlighted in Figures 2B and 2C also have significantly lower Tafel slopes than IrO_2 at potentials between 1.49 and 1.53 V. This may imply that the discharge of water occurs more readily on these electrode surfaces. The data also shows two compositions that behave similarly to IrO_2 in terms of the fluorescence intensity. These two compositions performed well in the stability studies discussed later. The Tafel slopes of these compositions more closely agree with the IrO_2 Tafel slopes at the lower overpotential value. The potential of each composition at 1 mA/cm^2 is also shown in the table. The potential is at least 15 mV lower for the two compositions that fluoresced more intensely than IrO_2. There is only a 5 mV difference in the potentials of the other two compositions that behave more like IrO_2. The second steps in the oxide path or electrochemical oxide path are both considered rate determining, with Tafel slopes of 30 mV/decade and 40 mV/decade, respectively. The Tafel slopes measured at potentials between 1.59 and 1.64 V are in agreement with literature reports of pure IrO_2 and RuO_2, which vary from 40 to 80 mV/decade.[8a,11,12b,20,21,22] Mixed

dx.doi.org/10.1021/co300086h | ACS Comb. Sci. 2013, 15, 82−89

oxides of Sn and Ir and Sn and Ru Tafel slopes have been reported in the range of 60−70 mV/decade for Sn concentrations of up to 50%.[9,11,12c] It is perhaps not prudent to discuss detailed mechanisms based on expected Tafel slopes without additional experiments including measurements over a large pH range, detecting reaction intermediates, or assessing surface oxidation states. However, because of the logarithmic current axis, presenting polarization curves in Tafel format allows for the comparison of different anode materials across a large range of current densities where performance at low current densities would be difficult to discern on a linear scale. A more detailed summary of all of electrochemical experiments and Tafel data can be found in Supporting Information, Tables S1 and S2.

The PGM mixed metal oxide electrodes were imaged with a scanning electron microscope (SEM) to gain an appreciation for the surface morphology. Images of several films are shown in Figure 4. Figure 4A is pure IrO_2. The presence of nanometer-size crystallites can be seen. This is not entirely unexpected since IrO_2 is not mixed with any other oxide and should be present as a single phase. Figure 4B shows a film of $Pt_{0.50}Pd_{0.50}$. Although some porosity is present in this film, no obvious electrocatalysis was seen during the screening experiments. This may highlight the fact that IrO_2 is required for reasonable electrocatalytic ability. Two of the more electrocatalytic films are shown in Figures 4C and 4D ($Ir_{0.42}Ru_{0.28}Pt_{0.05}Rh_{0.25}$ and $Ir_{0.20}Pt_{0.10}Rh_{0.70}$, respectively). As seen in the figures, the surfaces appear almost glassy, with very little roughness. Several very small bright spherical particles appear to pepper the surfaces; however, these were too small to image with the instrument. Both films have areas that appear as cracked mud. The image shows these fissures in the surface, and the FTO is visible beneath the films.

There appears to be very little difference in the surface morphology of the electrodes shown in Figures 4C and 4D. If efforts are undertaken to maximize the surface areas of these materials, it seems quite reasonable that even greater electrocatalytic activity could be realized. X-ray diffraction (XRD) analysis was not performed because of the thickness limitations of these printed electrodes.

Preliminary Stability Analysis. Stability studies were carried out on the most promising electrode compositions. The compositions chosen for stability studies all had current densities greater than 2.6 mA/cm^2 at a potential of 1.64 V in the polarization studies. Cyclic voltammetry was performed on one of these electrodes to determine the current density at a high potential (1.85 V vs NHE). The resulting current was 8.5 mA/cm^2, and 10 mA/cm^2 was chosen as the current density for stability studies. The current was held at 10 mA for a period of 30 min. The resulting curves are shown in Figure 5. The data indicate that three electrode compositions require a lower potential than the IrO_2 standard to achieve a current density of 10 mA/cm^2. Of these 3 compositions, 2 compositions ($Ir_{0.25}Pt_{0.25}Rh_{0.50}$ and $Ir_{0.20}Pt_{0.10}Rh_{0.70}$) have a noticeably smaller slope than the IrO_2 standard. The IrO_2 standard has a slope of 1.4 mV/min compared with 0.70 and 0.83 mV/min for the $Ir_{0.25}Pt_{0.25}Rh_{0.50}$ and the $Ir_{0.20}Pt_{0.10}Rh_{0.70}$ compositions, respectively. This may provide some insight as to the long-term stability of these electrode compositions compared to IrO_2. After analyzing the data, some trends are noticeable. All of the most promising compositions contain some amount of Rh. There are a few studies of oxides of rhodium, the majority limited to alkaline conditions,[23−27] none of which combine Rh

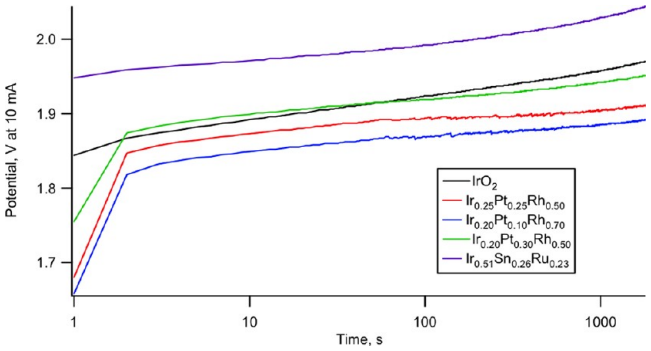

Figure 5. Stability studies of several promising compositions and the IrO_2 standard. As indicated in the graph, there are three compositions that appear to have both a greater catalytic activity based on potential and greater stability based on slope than the IrO_2 standard.

with any other catalytic metal for water electrooxidation. If only the potential at which a current density of 10 mA/cm^2 and the stability of the electrodes are taken into account, the compositions of the most promising catalysts contain only Ir, Pt, and Rh. However, two electrode compositions can be considered the most stable in terms of the slope of the overpotential loss in mV/min. These compositions both have slopes of 0.53 mV/min. The first composition is a simple binary containing $Ir_{0.60}Rh_{0.40}$. Perhaps more interesting is the second composition, a ternary containing $Ir_{0.50}Ru_{0.20}Rh_{0.30}$. Both of these compositions, despite their apparent stability advantage, require higher potentials than IrO_2 to maintain a 10 mA current (48 mV greater for the binary and 87 mV greater for the ternary). The cost of the ternary material should be lower than pure IrO_2, and this may offset the additional energy cost.

Only a few base metal compositions were subjected to stability studies. The Al compositions appeared to degrade with repeated cycling during the polarization studies. The best Nb compositions had current densities of less than 1.5 mA/cm^2 at 1.65 V and the stability was not studied. A composition containing Sn, Ir, and Ru, while performing similarly at low current densities to the IrO_2 standard, requires a relatively higher potential to achieve a 10 mA/cm^2 current density perhaps because of the insulating nature of undoped SnO_2. Additionally, no noticeable stability benefit of this composition was observed compared to the IrO_2 standard with both having slopes of 1.4 mV/min. The similarity in slope may be because Ir has been shown to migrate to the surface of Sn/Ir mixed oxides.[6,8b] When the Ir/Sn compositions contain greater than 10 mol percent Ir, others have found the mixed SnO_2/IrO_2 oxide behaves similarly to IrO_2. Hutchings investigated a ternary mixture of $Sn_{0.50}Ir_{0.25}Ru_{0.25}$ and found this composition exhibited greater stability than either IrO_2 or IrO_2/RuO_2 mixed oxides[6] whereas our catalyst, having a composition of $Ir_{0.51}Sn_{0.26}Ru_{0.23}$, does not reflect this behavior. Balko found that SnO_2/IrO_2 mixed metal oxide catalysts do not increase the lifetime of the catalyst.[11] The most obvious advantage of such a composition is the reduction in cost of the catalyst. Supporting Information, Table S3 contains data from additional stability studies.

CONCLUSIONS

We have demonstrated that a combinatorial approach for making mixed metal oxides in concert with a rapid screening method has been successful in finding water oxidation electrocatalysts that perform better in acidic conditions than a

pure IrO_2 standard. We have found that the addition of Rh appears to stabilize and/or enhance the water electrooxidation activity of IrO_2. The screening method developed herein may prove useful for distinguishing different water oxidation mechanisms and eventually produce electrocatalysts useful for water oxidation. Although the current density range studied herein is low when compared to that needed in a high performance electrolyzer, low surface area films were produced and considerable improvements in the apparent current densities would be gained by producing these materials in highly structured high surface area morphologies. Further studies on some of these promising materials with scale up to traditional catalyst nanopowders are warranted to verify their performance in an actual PEM electrolyzer. Although this paper describes many catalyst compositions, it is in no way a complete exploration of the vast number of possible electrocatalyst combinations.

■ ASSOCIATED CONTENT

Supporting Information

Detailed polarization data and stability studies. This material is available free of charge via the Internet at http://pubs.acs.org.

■ AUTHOR INFORMATION

Corresponding Author

*E-mail: bparkin1@uwyo.edu.

Funding

The authors gratefully acknowledge the Office of Energy Efficiency and Renewable Energy at the U.S. Department of Energy for its support for the work discussed in this paper under Grant DE-SC0004192.

Notes

The authors declare no competing financial interest.

■ ACKNOWLEDGMENTS

We thank Chris Capuano for helpful discussions and support.

■ REFERENCES

(1) Woodhouse, M.; Herman, G. S.; Parkinson, B. A. Combinatorial Approach to Identification of Catalysts for the Photoelectrolysis of Water. *Chem. Mater.* **2005**, *17*, 4318−4324.

(2) Woodhouse, M.; Parkinson, B. A. Combinatorial Discovery and Optimization of a Complex Oxide with Water Photoelectrolysis Activity. *Chem. Mater.* **2008**, *20*, 2495−2502.

(3) Reddington, E.; Sapienza, A.; Gurau, B.; Viswanathan, R.; Sarangapani, S.; Smotkin, E. S.; Mallouk, T. E. Combinatorial Electrochemistry: A Highly Parallel, Optical Screening Method for Discovery of Better Electrocatalysts. *Science* **1998**, *280*, 1735−1737.

(4) Trasatti, S. Electrocatalysis in the Anodic Evolution of Oxygen and Chlorine. *Electrochim. Acta* **1984**, *29*, 1503−1512.

(5) Loucka, T. The Reason for the Loss of Activity of Titanium Anodes Coated with a Layer of RuO_2 and TiO_2. *J. Appl. Electrochem.* **1977**, *7*, 211−214.

(6) Hutchings, R.; Muller, K.; Kotz, R.; Stucki, S. A Structural Investigation of Stabilized Oxygen Evolution Catalysts. *J. Mater. Sci.* **1984**, *19*, 3987−3994.

(7) Kotz, R.; Stucki, S. Stabilization of RuO_2 by IrO_2 for Anodic Oxygen Evolution in Acidic Media. *Electrochim. Acta* **1986**, *31*, 1311−1316.

(8) (a) Yeo, R. S.; Orehotsky, J.; Visscher, W.; Srinivasan, S. Ruthenium-Based Mixed Oxides as Electrocatalysts for Oxygen Evolution in Acidic Electrolytes. *J. Electrochem. Soc.* **1981**, *128*, 1900−1904 and. (b) Marshall, A. T.; Sunde, S.; Tsypkin, M.; Tunold, R. Performance of a PEM Water Electrolysis Cell Using $Ir_xRu_yTa_zO_2$ Electrocatalysts for the Oxygen Evolution Electrode. *Int. J. Hydrogen Energy* **2007**, *32*, 2320−2324.

(9) Gaudet, J.; Tavares, A. C.; Trasatti, S.; Guay, D. Physicochemical Characterization of Mixed RuO_2-SnO_2 Solid Solutions. *Chem. Mater.* **2005**, *17*, 1570−1579.

(10) Wu, X.; Scott, K. RuO_2 Supported on Sb-doped SnO_2 Nanoparticles for Polymer Electrolyte Membrane Water Electrolysis. *Int. J. Hydrogen Energy* **2011**, *36*, 5806−5810.

(11) Balko, E. N.; Nguyen, P. H. Iridium-Tin Mixed Oxide Anode Coatings. *J. Appl. Electrochem.* **1991**, *21*, 678−682.

(12) (a) Kotz, R.; Neff, H.; Stucki, S. Anodic Iridium Oxide Films. *J. Electrochem. Soc.* **1984**, *131*, 72−77. (b) De Pauli, C. P.; Trasatti, S. Electrochemical Surface Characterization of IrO_2 + SnO_2 Mixed Oxide Electrocatalysts. *J. Electroanal. Chem.* **1995**, *396*, 161−168. (c) De Pauli, C. P.; Trasatti, S. Composite Materials for Electrocatalysis of O_2 Evolution: IrO_2 + SnO_2 in Acid Solution. *J. Electroanal. Chem.* **2002**, *538*−*539*, 145−151.

(13) (a) Millet, P.; Alleau, T.; Durand, R. Characterization of Membrane-Electrode Assemblies for Solid Polymer Electrolyte Water Electrolysis. *J. Appl. Electrochem.* **1993**, *23*, 322−331. (b) Ioroi, T.; Kitazawa, N.; Yasuda, K.; Yamamoto, Y.; Takenaka, H. Iridium Oxide/Platinum Electrocatalysts for Unitized Regenerative Polymer Electrolyte Fuel Cells. *J. Electrochem. Soc.* **2000**, *147*, 2018−2022.

(14) Kadakia, K.; Datta, M. K.; Velikokhatnyi, O. I.; Jampani, P.; Park, S. K.; Saha, P.; Poston, J. A.; Manivannan, A.; Kumta, P. N. Novel (Ir,Sn,Nb)O_2 Anode Electrocatalysts with Reduced Noble Metal Content for PEM Based Water Electcrolysis. *Int. J. Hydrogen Energy* **2012**, *37*, 3001−3013.

(15) Dokoutchaev, A. G.; Abdelrazzaq, F.; Thompson, M. E.; Wilson, J.; Chang, C.; Bocarsly, A. Multicomponent Electrodes for Water Oxidation: From Combinatorial to Individual Electrode Study. *Chem. Mater.* **2002**, *14*, 3343−3348.

(16) Chen, G.; Bare, S. R.; Mallouk, T. E. Development of Supported Bifunctional Electrocatalysts for Unitized Regenerative Fuel Cells. *J. Electrochem. Soc.* **2002**, *149*, A1092−A1099.

(17) Gerken, J. B.; Chen, J. Y. C.; Masse, R. C.; Powell, A. B.; Stahl, S. S. Development of an O_2-Sensitive Fluorescence-Quenching Assay for the Combinatorial Discovery of Electrocatalysts for Water Oxidation. *Angew. Chem., Int. Ed.* **2012**, *51*, 6676−6680.

(18) Mori, H.; Sakamoto, K.; Mashito, S.; Matsuoka, Y.; Matsubayashi, M.; Sakai, K. Aerial Oxidation of Some 2-Pyridyl Ketone Hydrazones Catalyzed by Cu^{2+}. Physical Properties of Reaction Products. *Chem. Pharm. Bull.* **1993**, *41*, 1944−1947.

(19) Bockris, J. O'M. Kinetics of Activation Controlled Consecutive Electrochemical Reactions: Anodic Evolution of Oxygen. *J. Chem. Phys.* **1956**, *24*, 817−827.

(20) Rasten, E.; Hagen, G.; Tunold, R. Electrocatalysis in Water Electrolysis with Solid Polymer Electrolyte. *Electrochim. Acta* **2003**, *48*, 3945−3952.

(21) Marshall, A.; Borresen, B.; Hagen, G.; Tsypkin, M.; Tunold, R. Electrochemical Characterisation of $Ir_xSn_{1-x}O_2$ Powders as Oxygen Evolution Electorcatalysts. *Electrochim. Acta* **2006**, *51*, 3161−3167.

(22) Siracusano, S.; Baglio, V.; Di Blasi, A.; Briguglio, N.; Stassi, A.; Ornelas, R.; Trifoni, E.; Antonucci, V.; Arico, A. S. Electrochemical Characterization of Single Cell and Short Stack PEM Electrolyzers Based on Nanosized IrO_2 Anode Electrocatalyst. *Int. J. Hydrogen Energy* **2010**, *35*, 5558−5568.

(23) O'Sullivan, E. J. M.; Burke, L. D. Kinetics of Oxygen Gas Evolution on Hydrous Rhodium Oxide Films. *J. Electrochem. Soc.* **1990**, *137*, 466−471.

(24) Burke, L. D.; O'Sullivan, E. J. M. Enhanced Oxide Growth at a Rhodium Surface in Base Under Potential Cycling Conditions. *J. Electroanal. Chem.* **1978**, *93*, 11−18.

(25) Miles, M. H.; Huang, Y. H.; Srinivasan, S. The Oxygen Electrode Reaction in Alkaline Solutions on Oxide Electrodes Prepared by the Thermal Decomposition Method. *J. Electrochem. Soc.* **1978**, *125*, 1931−1934.

(26) Pallotta, C.; De Tacconi, N. R.; Arvia, A. J. Kinetics of the Oxygen Evolution Reaction on Rhodium Electrodes with Different Electrocatalytic Activity. *J. Electroanal. Chem.* **1981**, *122*, 367−372.
(27) Damjanovic, A.; Dey, A.; Bockris, J. O'M. Electrode Kinetics of Oxygen Evolutioin and Dissolution on Rh, Ir, and Pt-Rh Alloy Electrodes. *J. Electrochem. Soc.* **1966**, *113*, 739−746.